Tolerance Requirements for Dispersion Free Single-Mode Fiber Design: Influence of Geometrical Parameters, Dopant Diffusion, and Axial Dip

PIERRE-LUC FRANCOIS

Abstract—**The dispersion sensitivity to small changes in index-differences, radius, and wavelength is investigated in the case of dispersion free single-mode fibers. If a minimum bandwidth is required, tolerances on the various parameters can then be deduced: singly- and doubly-clad structures are compared. Constant reference is made to the HE_{11} mode spot-size to relate dispersion properties and attenuation. A nonzero fundamental mode cutoff is shown to induce an enhanced sensitivity to a change in fiber geometrical characteristics. The effect of dopant diffusion and axial dip on dispersion is then considered and conclusions are drawn concerning the use of profiles measured on preforms to predict fiber propagation properties.**

I. Introduction

SINCE the successful development of ultra-low loss fibers [1], [2], considerable interest was devoted to minimizing chromatic dispersion [3], [4], especially in the $\lambda = 1.55$ μm window. Singly-clad fibers with GeO_2-doped silica core were first used but high index-differences are then necessary to achieve zero dispersion; this was found to increase the fiber losses more than was expected by the increase in Rayleigh scattering with increasing germanium concentration [5]. Profiles with depressed cladding were then used to reduce the amount of GeO_2 in the core. With F/P_2O_5 doped inner-cladding, very low attenuation was again achieved [6]. The added degree of liberty introduced by this doubly-clad structure allowed minimizing the dispersion over a wide spectral range [7], [8]. In some cases, however [9], the fundamental mode has a nonzero cutoff resulting, as will be shown, in an enhanced dispersion sensitivity to any change in geometrical fiber parameters.

We derive a general expression for chromatic dispersion in the case of a multicomponent structure and apply it to fibers with GeO_2-doped silica core and F/P_2O_5 doped inner-cladding. Zero chromatic dispersion at $\lambda = 1.55$ μm is then considered in some details with constant reference to the HE_{11} mode spot-size, which governs splicing and microbending losses. The sensitivity of dispersion to changes in index-differences, radii, and operating wavelength is investigated; we also derive a very simple expression for the bandwidth X length product. The preceding results are then used to find tolerance requirements ensuring a given minimum fiber bandwidth.

Influence of dopant diffusion and axial dip on chromatic dispersion is then evaluated. The use of a slight change in geometrical parameters to compensate the effects of diffusion and dip is considered and conclusions are drawn concerning the use of refractive-index profiles measured on preforms to predict fiber propagation characteristics.

Manuscript received March 11, 1982; revised May 27, 1982.
The author is with CNET, Lannion, France.

II. Dispersion Free Fibers

A. Notations

Consider weakly guiding structures with depressed inner-cladding (Fig. 1), having a circular-symmetric refractive-index distribution $n(r)$

$$n^2(r) = n_o^2 + (n_1^2 - n_o^2) f_1(r) + (n_2^2 - n_o^2) f_2(r) \tag{1}$$

where

n_o = outer-cladding refractive-index (silica substrate)
n_1 = maximum refractive-index in the core
n_2 = minimum refractive-index in the inner-cladding
$f_1(r)$ and
$f_2(r)$ are profile functions corresponding to the core and inner-cladding, respectively, and take values between 0 and 1 [see Fig. 1(a), (b)].

The profile functions $f_1(r)$ and $f_2(r)$ are nonzero for $0 \leqslant r \leqslant a_1$ and $a_2 \leqslant r \leqslant b_2$; their actual shapes may be chosen to describe departures from a perfect step-index profile (dotted lines in Fig. 1) which always occur in practical fibers. In the subsequent discussion, axial dip and grading caused by dopant diffusion will be considered.

For future use, we define the following parameters.

Geometrical Parameters:

a = core radius of the undeformed step-index profile
b = inner-cladding radius of the undeformed step-index profile
$c = b/a$

$$\Delta_1 = \frac{n_1^2 - n_o^2}{2n_o^2};\quad \Delta_2 = \frac{n_2^2 - n_o^2}{2n_o^2} (\Delta_1, |\Delta_2| \ll 1)$$

$$\sigma = -\Delta_2/\Delta_1.$$

Mode Parameters:

$k = 2\pi/\lambda$, wave number in vacuum
$V = kan_o\sqrt{2\Delta_1} = ka\sqrt{n_1^2 - n_o^2}$ = normalized frequency
β = propagation constant of the HE_{11} fundamental mode
$W = a\sqrt{\beta^2 - k^2 n_o^2}$

$$B = \frac{\beta^2 - k^2 n_o^2}{k^2(n_1^2 - n_o^2)} = \frac{W^2}{V^2} = \text{normalized propagation constant} \tag{2}$$

0018-9480/82/1000-1478$00.75

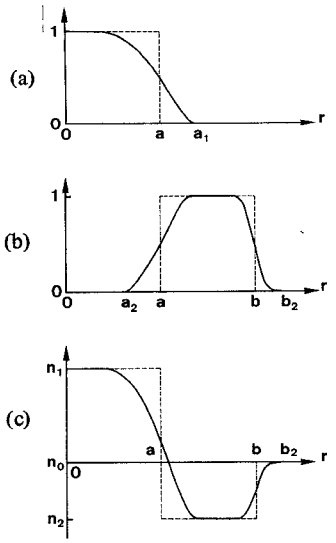

Fig. 1. Typical shape of profile functions used to describe dopant distribution in (a) the core and (b) inner-cladding; (c) refractive-index profile with diffused core and inner-cladding boundaries.

$$\Gamma_1 = \frac{\int_0^\infty f_1(r)\,\psi^2 r\,dr}{\int_0^\infty \psi^2 r\,dr};\quad \Gamma_2 = \frac{\int_0^\infty f_2(r)\,\psi^2 r\,dr}{\int_0^\infty \psi^2 r\,dr} \tag{3}$$

where $\psi(r)$, electric field distribution of the HE_{11} mode, is the solution of the scalar wave equation (under the weak guidance assumption) [10], [11]

$$\Delta_t\psi(r) + [k^2 n^2(r) - \beta^2]\,\psi(r) = 0 \tag{4}$$

or

$$\Delta_t\phi(u) + V^2\,[f_1(au) - \sigma f_2(au) - B]\,\phi(u) = 0 \tag{5}$$

with

$$u = r/a,\quad \phi(u) = \psi(au)$$

(Δ_t is the transverse part of the scalar Laplacian operator).

In most cases, more than two dopants are used in fiber fabrication and, in the weakly guiding case, (1) is generalized as [12]

$$n^2(r) = n_o^2 + \sum_{i=1}^{p} (n_i^2 - n_o^2) f_i(r) \tag{6}$$

where the summation is extended over p dopants.

As above, parameters Δ_i, $\sigma_i = -\Delta_i/\Delta_i (i \geq 2)$, and $\Gamma_i(3)$ may then be defined.

B. Dispersion in Multidopant Fibers

From (4) we deduce a variational expression for the propagation constant β [13]

$$\beta^2 = \frac{-\int_0^\infty |\nabla\psi|^2\,r\,dr + \int_0^\infty k^2 n^2(r)\,\psi^2 r\,dr}{\int_0^\infty \psi^2 r\,dr}. \tag{7}$$

Owing to the stationary property of this equation, partial derivation with respect to k yields

$$2\beta\frac{d\beta}{dk} = \frac{\int_0^\infty \frac{d}{dk}(k^2 n^2(r))\,\psi^2 r\,dr}{\int_0^\infty \psi^2 r\,dr}. \tag{8}$$

Substitution of (1) into (8) provides a relation between the effective index $n_e = \beta/k$ and group index $N_e = d\beta/dk = d(kn_e)/dk$ of the mode and the group indexes $N_i = d(kn_i)/dk$, $i = 0, 1, 2$

$$n_e N_e = n_o N_o + (n_1 N_1 - n_o N_o)\,\Gamma_1 + (n_2 N_2 - n_o N_o)\,\Gamma_2. \tag{9}$$

The transit time per unit length $\tau(\lambda)$ of a mode is equal to $\tau(\lambda) = N_e/c_o$ (c_o is the light velocity in vacuum) and may be expanded as a Taylor series about the mean wavelength λ_s of the source

$$\tau(\lambda) = \tau(\lambda_s) + (\lambda - \lambda_s)\left.\frac{d\tau}{d\lambda}\right|_{\lambda_s} + \frac{(\lambda - \lambda_s)^2}{2}\frac{d^2\tau}{d\lambda^2}. \tag{10}$$

The dispersion coefficient $D_1 = d\tau/d\lambda$ is then equal to

$$D_1 = \frac{d\tau}{d\lambda} = \frac{1}{c_o}\frac{dN_e}{d\lambda} = -\frac{\lambda}{c_o}\left.\frac{d^2 n_e}{d\lambda^2}\right|_{\lambda_s}. \tag{11}$$

Differentiation of (9) with respect to wavelength yields the expression for D_1

$$D_1 = s_m + s_w + s_{mw} \tag{12}$$

with

$$s_m = -\frac{\lambda}{c_o}\,[n_o'' + (n_1'' - n_o'')\,\Gamma_1 + (n_2'' - n_o'')\,\Gamma_2] \tag{12}'$$

$$s_w = -\frac{n_o\Delta_1}{\lambda c_o}\left[2B + 2\left(V\frac{d\Gamma_1}{dV} - \Gamma_1\right) - 2\sigma\left(V\frac{d\Gamma_2}{dV} - \Gamma_2\right)\right] \tag{12}''$$

$$s_{mw} = \frac{1}{c_o}\left[(n_1' - n_o')\left(2V\frac{d\Gamma_1}{dV} - \sigma V\frac{d\Gamma_2}{dV}\right) + (n_2' - n_o')\,V\frac{d\Gamma_2}{dV}\right] \tag{12}'''$$

where the prime indicates differentiation with respect to wavelength.

The assumption of weak guidance was used throughout and only first order terms in index-differences or their derivatives were retained.

A simplification of (12) is possible when using a relation existing between Γ_1, Γ_2, σ, and B. From the definition (2) of B, one can express β^2 as

$$\beta^2 = k^2\,[n_o^2 + (n_1^2 - n_o^2)\,B]. \tag{13}$$

Assuming, for our particular purpose, n_o and n_1 to be independent of wavelength, we obtain by differentiation of (13) with respect to k the following expression for $n_e N_e$

$$n_e N_e = \frac{\beta}{k}\frac{d\beta}{dk} = n_o^2 + (n_1^2 - n_o^2)\,\frac{1}{2}\left(\frac{d(VB)}{dV} + B\right). \tag{14}$$

With the same assumption, (9) reads

$$n_e N_e = n_o^2 + (n_1^2 - n_o^2)\,\Gamma_1 + (n_2^2 - n_o^2)\,\Gamma_2 = n_o^2 + (n_1^2 - n_o^2)\,[\Gamma_1 - \sigma\Gamma_2]. \quad (15)$$

Identification of (14) and (15) yields the relation

$$\Gamma_1 - \sigma\Gamma_2 = \frac{1}{2}\left(\frac{d(VB)}{dV} + B\right). \quad (16)$$

Using (16), the expression for D_1 may then be rewritten as

$$D_1 = s_m + s_w + s_{mw} \quad (17)$$

with

$$s_m = -\frac{\lambda}{c_o}\,[n_o'' + (n_1'' - n_o'')\,\Gamma_1 + (n_2'' - n_o'')\,\Gamma_2] \quad (17)'$$

$$s_w = -\frac{n_o \Delta_1}{\lambda c_o}\,V\frac{d^2(VB)}{dV^2} \quad (17)''$$

$$s_{mw} = \frac{1}{c_o}\left[\frac{n_1' - n_o'}{2}\left(V\frac{d^2(VB)}{dV^2} + \frac{d(VB)}{dV} - B\right) + (n_1' - n_o')\,V\frac{d\Gamma_1}{dV} + (n_2' - n_o')\,V\frac{d\Gamma_2}{dV}\right]. \quad (17)'''$$

The material dispersion term s_m $(17)'$ is equal to a weighted average of the material dispersions of silica and of dopants 1 and 2, with weights $1-\Gamma_1-\Gamma_2$, Γ_1 and Γ_2. From (3), Γ_1 and Γ_2 are always smaller or equal to the fractions of the total power which travel in the core and the inner-cladding, respectively; there is equality only in the ideal case of a perfect step-index profile. The waveguide dispersion term s_w $(17)''$ depends only on B and has exactly the same expression as in singly-clad structures [14]. The last term s_{mw} $(17)'''$ is the so-called composite dispersion [14].

In the case of a uniform cladding, $n_2 = n_o$, $\sigma = -\Delta_2/\Delta_1 = 0$, and $\Gamma_2 = 0$. With these simplifications, substitution of (16) into (17) gives expressions for s_m, s_w, and s_{mw} which only depend on the normalized propagation constant B and are exactly identical to previously published ones [14].

In the case of more than two dopants, s_w keeps the same expression $(17)''$, but $(17)'$ and $(17)'''$ may be generalized as

$$s_m = -\frac{\lambda}{c_o}\left[n_o'' + \sum_{i=1}^{p}(n_i'' - n_o'')\,\Gamma_i\right] \quad (18)$$

$$s_{mw} = \frac{1}{c_o}\left[\frac{n_1' - n_o'}{2}\left(V\frac{d^2(VB)}{dV^2} + \frac{d(VB)}{dV} - B\right) + \sum_{i=1}^{p}(n_i' - n_o')\,V\frac{d\Gamma_i}{dV}\right] \quad (18)'$$

where the summation is extended over p dopants.

The dominant term in (18) is the silica material dispersion $s_{mo} = -\lambda n_o''/c_o$ equal to 21.9 ps/(km · nm) at $\lambda = 1.55$ μm. The composite dispersion s_{mw} is often neglected (s_{mw} in order of 0.1 ps/km · nm), but nevertheless was retained in our calculations.

C. Dispersion Free Fiber Design

We consider only the best candidate for dispersion free propagation in the $\lambda = 1.55$ μm ultra-low loss window: it seems to be a fiber composed of a GeO_2-doped SiO_2 core and a P_2O_5/F-doped SiO_2 cladding [6]-[8]. We are thus here in the case of a three-dopant structure. A small germanium concentration and a low drawing temperature were shown to be two essential conditions to achieve low losses with fibers made by MCVD [5]. Fluorine doping creates a depressed inner-cladding which allows zero dispersion to be obtained with a reduced amount of germanium in the core.

P_2O_5 allows a reduction of the drawing temperature and is always introduced in very small quantities (concentration kept below 0.2 mole percent). We shall thus neglect the action of P_2O_5 in the calculation of dispersion.

Dispersion data are available in the literature for only a small number of dopant concentrations, but values of n, n', and n'', for any concentrations may, however, be obtained by interpolation. We used the Sellmeier expansion to compute the indexes and their derivatives

$$n^2 - 1 = \sum_{i=1}^{3}\frac{A_i\lambda^2}{(\lambda^2 - \lambda_i^2)}. \quad (19)$$

The interpolations were made between the values of n, n', or n'' corresponding to pure silica, 5.8 mole percent GeO_2-doped silica and 1.0 mole percent F-doped silica [15].

Consider first the case of a perfect step-index profile [dotted line in Fig. 1(c)] with a radii ratio $c = b/a = 2$. Using $\sigma = -\Delta_2/\Delta_1$ as a parameter, the core radius a_o for zero total dispersion at $\lambda = 1.55$ μm was obtained as a function of the normalized index-difference Δ_1; the result corresponds to the curves in dotted lines in Fig. 2. For a given value of Δ_1, a_o increases with σ and, for each σ, a_o remains smaller than a maximum value as Δ_1 varies. A comparison between the dotted curves $\sigma = 0$ and $\sigma > 0$ of Fig. 2 shows that zero dispersion for a singly-clad profile ($\sigma = 0$) requires larger Δ_1 and smaller core radii than for profiles with depressed inner-cladding ($\sigma > 0$).

The curves in full lines in Fig. 2 give the value of the HE_{11} mode spot-size ω, as a function of Δ_1 and for the core radius a_o corresponding to the zero dispersion condition. Marcuse's definition of ω was adopted [16], [17]. In the weak guidance assumption, the HE_{11} field distribution is nearly Gaussian in shape and can be approximated by

$$G(r, \omega) = \frac{2}{\omega\sqrt{2\pi}}\,e^{-(r/\omega)^2}. \quad (20)$$

The mode spot-size ω is then the width parameter of the Gaussian distribution $G(r, \omega)$ which has the maximum launching efficiency into the actual HE_{11} mode. In Fig. 3, values of ω/a are reported and correspond to the profiles considered in Fig. 2. The fundamental mode cutoff V-values are zero for $\sigma = 0$ and $\sigma = 0.2$, but are 0.766, 1.253, and 1.441 for $\sigma = 0.4$, 0.6, and 0.8, respectively. As is shown in Fig. 3, ω/a increases dramatically as the HE_{11} mode approaches its cutoff. For higher values of $V = ka n_o\sqrt{2\Delta_1}$, ω/a decreases when σ increases; far from cutoff, the mode sees an index-difference equal to $\Delta_1 - \Delta_2 = \Delta_1(1 + \sigma)$ and an increase in σ leads to a

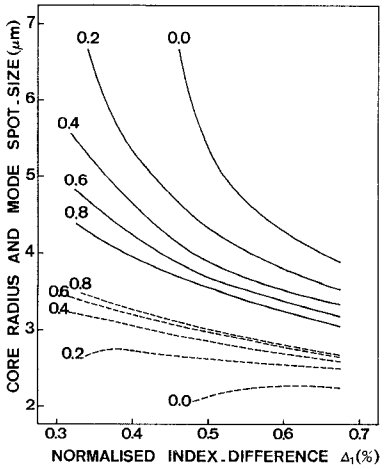

Fig. 2. Radius (dotted lines) and HE_{11} mode spot-size (full lines) of dispersion free fibers at $\lambda = 1.55$ μm, as a function of the normalized index-difference Δ_1 in the core. Labeling parameter is $\sigma = -\Delta_2/\Delta_1$.

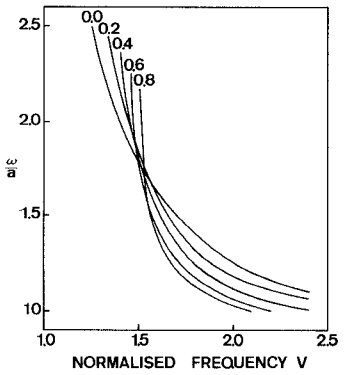

Fig. 3. Normalized HE_{11} mode spot-size as a function of $V = ka n_o \sqrt{2\Delta_1}$. Labeling parameter is $\sigma = -\Delta_2/\Delta_1$.

tighter field confinement to the core, corresponding to a smaller value of ω/a.

The splicing and microbending losses are mainly determined by the mode spot-size. Realistic values of ω cover the range 4-6 μm [18]. Fig. 2 then indicates the interval in which Δ_1 should be chosen; for a given value of ω, on the other hand, the normalized index-difference Δ_1 corresponding to zero dispersion decreases as σ increases. We recall that, ω being fixed, a decrease in Δ_1 allows a smaller attenuation for the fiber because of the smaller excess loss caused by GeO_2 in this case. However, σ should not be chosen too large since, in this case, the HE_{11} mode operates very near its cutoff and the tolerances on the fiber structural parameters become very narrow.

III. Tolerance Requirements

The two dominant terms in the expression (17) for the coefficient D_1 are the material dispersion $s_{mo} = -\lambda n_o''/c_o$ of silica and the waveguide dispersion s_w (17)'' ($s_{mo} \simeq 21.9$ ps/(km · nm) at $\lambda = 1.55$ μm). Zero dispersion corresponds approximately to the relation

$$\Delta_1 V \frac{d^2(VB)}{dV^2} = \frac{\lambda c_o}{n_o} s_{mo}. \tag{21}$$

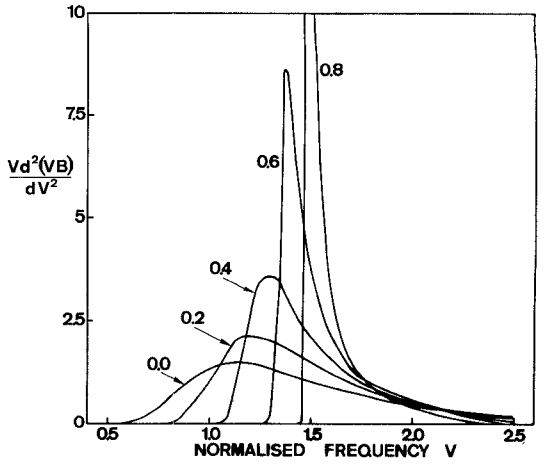

Fig. 4. Variation of the waveguide dispersion coefficient as a function of $V = ka n_o \sqrt{2\Delta_1}$. Labeling parameter is $\sigma = -\Delta_2/\Delta_1$.

In Fig. 4, $V d^2(VB)/dV^2$ is displayed as a function of V, for the profiles already considered in the preceding section (i.e., $c = b/a = 2$ and $\sigma = -\Delta_2/\Delta_1 = 0, 0.2, 0.4, 0.6, 0.8$). Owing to a nonzero fundamental mode cutoff, high values and quick variations of this parameter are observed in cases $\sigma = 0.4, 0.6$, and 0.8. The condition for zero dispersion may thus be obtained with a value of Δ_1 smaller than in cases $\sigma = 0$ or 0.2 [see (21)], but because of the very steep slopes of the curves, the sensitivity to a small change of parameters then becomes very strong. Note that (21) was only introduced to explain intuitively the origin of the enhanced sensitivity of the profiles with deep inner-cladding; in our calculations of dispersion, all the terms appearing in (17)' and (17)'' are retained.

A. Sensitivity to a Change of Parameters

The parameters are the normalized index-differences Δ_1 and Δ_2, the radii a and b, and the wavelength of operation λ. Δ_1, Δ_2, a, and b are chosen so that the wavelength λ_0 for zero dispersion coincides with the mean wavelength λ_s of the source. These parameters can be obtained from Fig. 2 for $\lambda_s = \lambda_0 = 1.55$ μm and $c = b/a = 2$. About these values, D_1 may be expanded as

$$D_1 = \frac{\delta D_1}{\delta \Delta_1} d\Delta_1 + \frac{\delta D_1}{\delta \Delta_2} d\Delta_2 + \frac{\delta D_1}{\delta a} da + \frac{\delta D_1}{\delta b} db + \frac{\delta D_1}{\delta \lambda} d\lambda. \tag{22}$$

The sensitivity coefficients $\delta D_1/\delta\Delta_1$ and $\delta D_1/\delta\Delta_2$ are displayed in Fig. 5(a). For example, when $\sigma = 0.2$ and $\Delta_1 = 0.425$ percent, which corresponds to a HE_{11} mode spot-size $\omega = 5$ μm (see Fig. 2), $\delta D_1/\delta\Delta_1$ and $\delta D_1/\delta\Delta_2$ are equal, respectively, to 30 and 95 ps/(km · nm · percent); a 10 percent increase in Δ_1 and Δ_2, corresponding to $d\Delta_1 = 0.425 \times 0.1 \simeq 0.0425$ percent and $d\Delta_2 = 0.425 \times 0.2 \times 0.1 = 0.0085$ percent ($d\Delta_1$ and $d\Delta_2$ are expressed in absolute index-difference percentages), will increase the dispersion from $D_1 = 0$ to $D_1 = 1.28$ and 0.81 ps/(km · nm). For the interesting values of Δ_1, $\delta D_1/\delta\Delta_1$ and $\delta D_1/\delta\Delta_2$ are positive for $\sigma \geqslant 0.2$; in the particular case of a singly-clad profile ($\sigma = 0$), $\delta D_1/\delta\Delta_1$ is negative

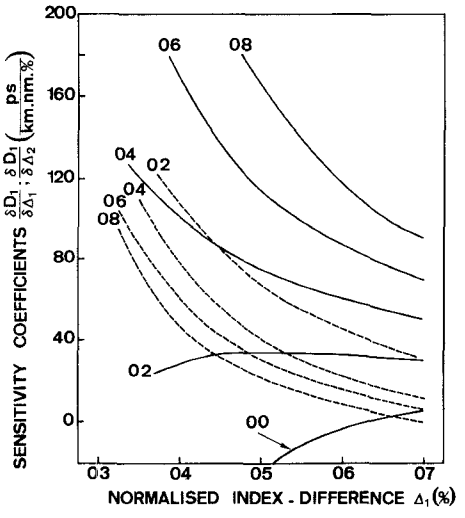

(a)

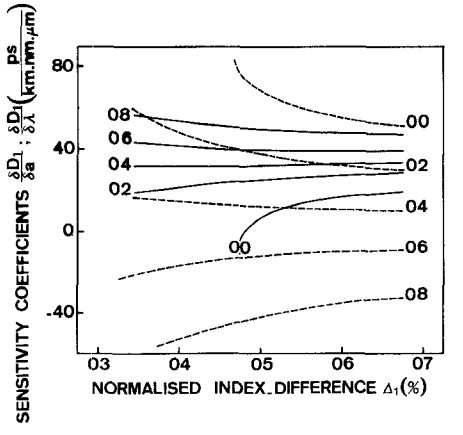

(b)

Fig. 5. Sensitivity of dispersion to small changes of parameters. (a) Index-differences Δ_1 (full lines) and Δ_2 (dotted lines). (b) Core radius a (full lines) and wavelength λ (dotted lines). Labeling parameter is $\sigma = -\Delta_2/\Delta_1$.

for $\Delta_1 \leqslant 0.64$ percent and increasing Δ_1 shifts the dispersion towards negative values. For a fixed Δ_1 and increasing σ values, $\delta D_1/\delta\Delta_1$ increases, but $\delta D_1/\delta\Delta_2$ decreases. However, for smaller values of Δ_1, the mode approaches its cutoff and $\delta D_1/\delta\Delta_2$ also increases with σ.

Fig. 5(b) shows values of $\delta D_1/\delta a$ and $\delta D_1/\delta\lambda$; $\delta D_1/\delta b$ is always small ($|\delta D_1/\delta b| < 10$ ps/(km · nm · μm)) and we did not report it. $\delta D_1/\delta a$ increases with σ and is positive; as σ increases, $\delta D_1/\delta\lambda$ decreases from some positive value, is equal to zero for a σ-value between 0.4 and 0.6, and assumes very large negative values as σ further increases.

An obvious conclusion is that too high values of σ are not of practical use since they correspond to a high nonzero fundamental mode cutoff and thus to an enhanced sensitivity to any change of parameters. Kawakami expressed the condition for zero HE_{11} mode cutoff by the fact that the "average" refractive index in the core and inner-cladding must be positive. With our notations, this condition can be written as

$$\sigma \leqslant \frac{1}{c^2 - 1}. \tag{23}$$

In the case under consideration, this corresponds to $\sigma \leqslant \frac{1}{3}$. The singly-clad profile ($\sigma = 0$) has the smallest sensitivity (except for wavelength), but high Δ_1 values are required for zero dispersion; for a given ratio $c = b/a$, the values of σ realizing the best tradeoff are thus located near $\sigma = 1/(c^2 - 1)$.

B. Tolerances

In a recent paper [19], Cohen *et al.* reported an expression for the baseband power transfer function $H_c(w)$ which, in the case of a Gaussian power spectrum for the light source, can be rewritten as

$$|H_c(w,\lambda)| = \frac{1}{\sqrt[4]{1 + \left(zw\,\frac{\sigma_s^2}{4}\left|\frac{\delta D_1}{\delta\lambda}\right|\right)^2}} \cdot \exp\left\{-\frac{\left(zw\frac{\sigma_s}{2}|D_1|\right)^2}{2\left[1 + \left(zw\,\frac{\sigma_s^2}{4}\left|\frac{\delta D_1}{\delta\lambda}\right|\right)^2\right]}\right\} \tag{24}$$

where

- z is the length along the fiber
- w is the radian baseband frequency
- σ_s is the full rms spectral width of the source, assuming a Gaussian shape for the laser power spectrum envelope [19].

The 3 dB optical bandwidth corresponds to $|H_c(w,\lambda)| = 0.5$ and can be approximated by two very simple expressions.

1) At the Zero Dispersion Wavelength $\lambda = \lambda_0$:

$$BW = \frac{zw}{2\pi} \simeq \frac{2.47\,10^6}{\sigma_s^2\left|\frac{\delta D_1}{\delta\lambda}\right|}\ \text{GHz} \cdot \text{km} \tag{25}$$

where $\delta D_1/\delta\lambda$ is expressed in ps/(km · nm · μm) and σ_s in nm.

BW, given by (25), corresponds to the peak of the bandwidth spectra and is inversely proportional to σ_s^2.

2) $\lambda \neq \lambda_0$:

$$BW \simeq \frac{375}{\sigma_s|D_1|}\ \text{GHz} \cdot \text{km}. \tag{26}$$

Away from the zero dispersion wavelength, the bandwidth diminishes very quickly and is inversely proportional to σ_s.

To precise tolerance requirements for the various parameters, we assume that Δ_1, Δ_2, a, and λ are centered random variables with uniform probability laws; the rms deviations σ_{Δ_1}, σ_{Δ_2}, σ_a, and σ_λ are then equal, respectively, to $\delta\Delta_1/\sqrt{3}$, $\delta\Delta_2/\sqrt{3}$, $\delta a/\sqrt{3}$, $\delta\lambda/\sqrt{3}$ where δx denotes the tolerance on the variable x($x = \Delta_1, \Delta_2, a$, or λ). The rms deviation of the total dispersion D_1 is then

$$\sigma_{D_1} = \left(\sum_{x=\Delta_1,\Delta_2,a,\lambda}\left(\frac{\delta D_1}{\delta x}\right)^2\left(\frac{\delta x}{\sqrt{3}}\right)^2\right)^{1/2}. \tag{27}$$

For simplicity sake, we assume that, for $x = \Delta_1, \Delta_2, a$, and λ, all the terms $(\delta D_1/\delta x)^2\,(\delta x)^2$ are equal. Substitution of σ_{D_1} for $|D_1|$ in (26) then gives

$$\left|\frac{\delta D_1}{\delta x}\right| \cdot \delta x = \frac{375}{\sigma_s BW}\sqrt{\frac{3}{4}}. \tag{28}$$

Assume a spectral width $\sigma_s = 5$ nm for the laser source; if we require, for example, that $BW > 25$ GHz · km, then the tolerance δx is determined by the relation

$$\left|\frac{\delta D_1}{\delta x}\right| \delta x = 2.6 \text{ ps/(km} \cdot \text{nm)} \quad \text{for} \quad x = \Delta_1, \Delta_2, a, \lambda. \tag{29}$$

As an illustration, Table I reports values of $\delta\Delta_1$, $\delta\Delta_2$, δa, and $\delta\lambda$ in the case of a dispersion free fiber with $c = 2$, a mode spot-size $\omega = 5$ μm and for $\sigma = 0$, 0.2, 0.4, and 0.6. Singly-clad fibers ($\sigma = 0$) are less sensitive to radius or Δ_1 changes than profiles with depressed-cladding but the wavelength tolerances are smaller. During the fabrication, the routine accuracy on the parameters is about 10 percent on normalized index-differences and 5 percent on radii. For $c = 0.2$, $\delta\Delta_1/\Delta_1 = 19$ percent, and $\delta a/a = 4$ percent; for $c = 0.4$, $\delta\Delta_1/\Delta_1 = 6$ percent and $\delta a/a = 2.6$ percent. Special attention should then be devoted to control core radius and also, as σ increases, index-differences.

In the example under consideration, the maximum theoretical bandwidths (25) at zero dispersion are equal to 1.5 10^3 GHz · km, 2.3 10^3 GHz · km, 6.6 10^3 GHz · km, and 4.10^3 GHz · km for $\sigma = 0$, 0.2, 0.4, and 0.6, respectively. This confirms that there is no interest at all to choose too high a value for σ and that any departure from the parameter values achieving zero dispersion drastically reduces the bandwidth (from about 3.10^3 GHz · km to 25 GHz · km for the variations of Table I).

With the aid of (28) and Figs. 2 and 5(a), (b), the reader may consider other particular cases; we only stress the importance of a small source spectral width σ_s. With a monochromatic source, the tolerances are of course much relaxed.

C. Shift of Zero Dispersion Wavelength λ_0

For given changes $d\Delta_1$, $d\Delta_2$, da around the parameter values achieving zero dispersion, the shift of λ_0 can be obtained from (22) and the results of Fig. 5(a) and (b)

$$\delta\lambda = \lambda_0' - \lambda_0 = -\frac{1}{\dfrac{\delta D_1}{\delta\lambda}}\left\{\frac{\delta D_1}{\delta\Delta_1}d\Delta_1 + \frac{\delta D_1}{\delta\Delta_2}d\Delta_2 + \frac{\delta D_1}{\delta a}da\right\}. \tag{30}$$

When the derivatives of D_1 assume positive values, an increase in any among the three parameters Δ_1, Δ_2, a leads to a decrease in λ_0. It is also possible to evaluate, at least qualitatively, the difference in λ_0 between a perfect step-index profile and a slightly deformed one: an equivalent step-index profile with parameters Δ_1', Δ_2', a' can be defined for any kind of deformation [20], [21] and (30) is then applied with $d\Delta_1 = \Delta_1' - \Delta_1$, $d\Delta_2 = \Delta_2' - \Delta_2$, $da = a' - a$ (we neglect the effect of a variation in inner-cladding radius b).

Profile measurements on preforms can indicate departures $d\Delta_1$, $d\Delta_2$ from the Δ_1 and Δ_2 values required to achieve zero dispersion at a given wavelength λ_0. To maintain zero dispersion at $\lambda = \lambda_0$, the fiber must be pulled with a radius equal to $a = a_0 + \delta a$ where

$$\delta a = -\frac{1}{\dfrac{\delta D_1}{\delta a}}\left\{\frac{\delta D_1}{\delta\Delta_1}d\Delta_1 + \frac{\delta D_1}{\delta\Delta_2}d\Delta_2\right\}. \tag{31}$$

Of course, such a correction is no longer possible for values of δa smaller than the accuracy achievable on the radius a.

TABLE I

TOLERANCE REQUIREMENTS FOR A FIBER BANDWIDTH LARGER OR EQUAL TO 25 GHz · km AND A SOURCE SPECTRAL WIDTH $\sigma_s = 5$ nm. THE ZERO DISPERSION WAVELENGTH IS $\lambda_0 = 1.55$ μm FOR THE VALUES OF Δ_1, Δ_2, AND a REPORTED ($\sigma = -\Delta_2/\Delta_1$ AND $c = b/a = 2$). THE HE_{11} MODE SPOT-SIZE IS EQUAL TO $\omega = 5$ μm. Δ_1, Δ_2, $\delta\Delta_1$, $\delta\Delta_2$ ARE EXPRESSED IN PERCENTS AND a, δa, $\delta\lambda$ IN MICRONS.

σ	0.	0.2	0.4	0.6
Δ_1	0.52	0.43	0.37	0.31
Δ_2	0.00	- 0.086	- 0.148	- 0.186
a	2.2	2.7	3.1	3.5
$\delta\Delta_1$	0.13	0.08	0.023	0.005
$\delta\Delta_2$	-	0.028	0.027	0.022
δa	0.17	0.11	0.08	0.06
$\delta\lambda$	0.04	0.06	0.17	0.1

IV. Effect of Dopant Diffusion and Axial Dip

A. Models Used

The dopant diffusion is usually described by an exponential law. For convenience sake, we describe the effect in a somewhat different way. We assume profile functions $f_1(r)$ and $f_2(r)$ [see (1)] having the following expressions.

- For the core region

$$f_1(r) = \frac{1}{2}\left[1 + \cos\left\{\pi\left(\frac{r}{a_1}\right)^{2\alpha_1}\right\}\right], \qquad r \leqslant a_1$$
$$= 0 \qquad a_1 < r \tag{32}$$

where a_1, α_1 are adjustable parameters.

- For the inner-cladding region

$$f_2(r) = \frac{1}{2}\left[1 + \cos\left\{\pi\left(\frac{r^2 - c^2}{u^2}\right)^{\alpha_2}\right\}\right], \qquad a_2 \leqslant r \leqslant b_2$$
$$= 0 \qquad r < a_2 \text{ or } b_2 < r \tag{33}$$

where

$$c^2 = \frac{a^2 + b^2}{2}$$

$$u^2 = \frac{b_2^2 - a_2^2}{2}$$

$$b_2^2 = a^2 + b^2 - a_2^2$$

where a_2, α_2 are adjustable parameters.

A perfect step-index profile [dotted lines on Fig. 1(a), (b)]

corresponds to $\alpha_1 = \infty$ or $\alpha_2 = \infty$. For $\alpha_1 < \infty$ and $\alpha_2 < \infty$, $f_1(r)$ and $f_2(r)$ assume the general shape displayed in Fig. 1(a) and (b) (full lines). The core dopants diffusion into the inner-cladding stops at a distance $a_1 > a$ from the center; the inner-cladding dopants penetrate into the core region as far as $r = a_2 < a$. Note that dopants situated at $r = \sqrt{(a^2 + b^2)/2}$ do not migrate. The exponants α_1 and α_2 are determined by expressing that the quantity of dopants is conserved during the diffusion process; the integrals $\int_0^\infty f_1(r) r\, dr$ and $\int_0^\infty f_2(r) r\, dr$ must remain constant as a_1 or a_2 varies and $\alpha_1(a_1)$, $\alpha_2(a_2)$ are obtained by solving the following two equations for α_1 and α_2:

$$1 + \frac{1}{2} \sum_{j=1}^{\infty} \frac{(-1)^j}{(2j)!} \frac{\pi^{2j}}{2j\alpha_1 + 1} = \left(\frac{a}{a_1}\right)^2 \tag{34}$$

$$1 + \frac{1}{2} \sum_{j=1}^{\infty} \frac{(-1)^j}{(2j)!} \frac{\pi^{2j}}{2j\alpha_2 + 1} = \frac{b^2 - a^2}{b_2^2 - a_2^2}. \tag{35}$$

The choice of α_1 and α_2 as parameters describing the diffusion would have lead to a very simple determination of a_1 and a_2 by (34), (35); we adopt here a_1 and a_2 as leading parameters because of their more obvious physical significations.

The axial dip was modeled by a power law

$$\begin{aligned} f_1(r) &= 1 - \gamma \left[1 - \frac{r}{a_d}\right]^{\alpha_d}, && 0 \leqslant r \leqslant a_d \\ &= 1, && a_d < r \leqslant a \\ &= 0, && a < r \end{aligned} \tag{36}$$

where γ is the depth of the dip and a_d is the dip radius.

The corresponding profile has the shape displayed in Fig. 6.

For these two departures from a perfect step-index, the scalar wave equation (4) was solved by a numerical method described recently [22]. We tested this method in the case of step-index profiles with depressed inner-cladding: the parameters which determine the procedure accuracy were chosen to ensure a five figure precision on the normalized propagation constant and its first two derivatives.

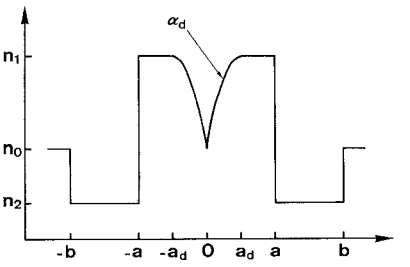

Fig. 6. Profile with axial dip.

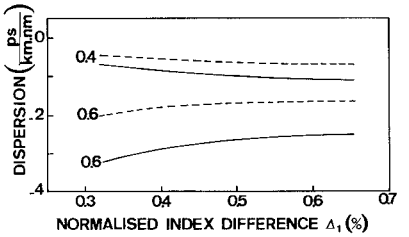

Fig. 7. Change of dispersion in case of inner-cladding dopant diffusion into the core (33) with $a_2 = 0.6a$ (dotted lines) and $a_2 = 0.4a$ (full lines). Labeling parameter is $\sigma = -\Delta_2/\Delta_1$.

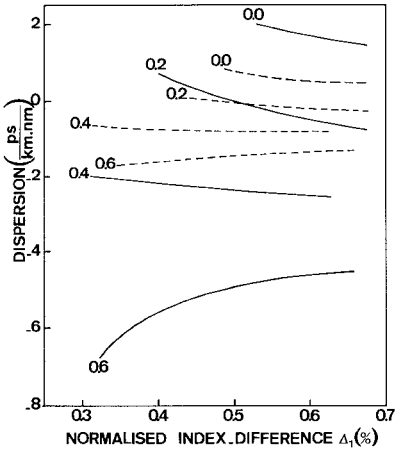

Fig. 8. Change of dispersion in case of core dopant diffusion into the inner-cladding (32) with $a_1 = 1.2a$ (dotted lines) and $a_1 = 1.4a$ (full lines). Labeling parameter is $\sigma = -\Delta_2/\Delta_1$.

B. Results

We consider dispersion free step-index profiles with depressed-cladding and investigate the dispersion variation caused by diffusion or axial dip.

In the case of diffusion into the core of inner-cladding dopants, no marked effect was observed as long as $a_2 > 0.6a$ and, for a given a_2, the effect was found to increase with $\sigma = -\Delta_2/\Delta_1$. In Fig. 7, results are reported for $a_2 = 0.6a$ (dotted lines) and $a_2 = 0.4a$ (full lines); labeling parameters indicate the value of σ. For σ smaller than 0.2, the change of dispersion was always negligeable.

Core dopants diffusion into the inner-cladding is found to have more effect. The results are shown in Fig. 8 for $a_1 = 1.2a$ (dotted line) and $a_1 = 1.4a$ (full line). Two behaviors can be observed. For $\sigma = 0$, the diffusion causes a positive dispersion D_1 and an increase in a_1 yields increasing positive values for D_1. If $\sigma \geqslant 0.4$, then $D_1 < 0$ and increasing a_1 gives increasing negative values of dispersion. $\sigma = 0.2$ corresponds to an intermediate case in which the two behaviors are observed on each side of a point where $D_1 = 0$ for both $a_1 = 1.2a$ and $1.4a$ ($\Delta_1 = 0.51$ percent, $\sigma = 0.2$ on Fig. 8). With the notations of Section III-C the case under consideration corresponds to $d\Delta_1 = \Delta_1' - \Delta_1 \leqslant 0$. When $\sigma = 0$, then $\delta D_1/\delta\Delta_1 < 0$ [see Fig. 5(a)] which explains the positive dispersion observed in Fig. 8 (see (22) for D_1). If $\sigma \geqslant 0.4$, then $\delta D_1/\delta\Delta_1 > 0$ and the dispersion assumes negative values.

The dispersion variations caused by an axial dip are shown in Fig. 9 when $\alpha_d = 2$, $\gamma = 1$ and for $a_d = 0.5a$ (dotted lines) and $a_d = a$ (full lines). As in Fig. 9, two behaviors are observed and depend on the sign of $\delta D_1/\delta\Delta_1$.

So far, we considered only the mode dispersion properties.

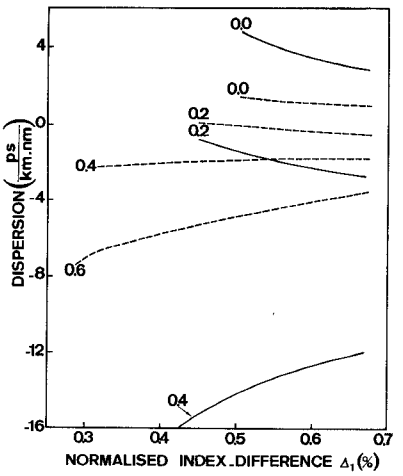

Fig. 9. Change of dispersion in case of axial dip (36) with $a_d = 0.5a$ (dotted lines) and $a_d = a$ (full lines). Labeling parameter is $\sigma = -\Delta_2/\Delta_1$, ($\alpha_d = 2, \gamma = 1$).

TABLE II
HE_{11} AND TE_{01} MODE CUTOFF V-VALUES

σ		I	II a_2/a		III a_1/a		IV a_d/a	
			0.6	0.4	1.2	1.4	0.5	1.0
0.0	HE_{11}	0.000	-	-	0.000	0.000	0.000	0.000
	TE_{01}	2.405	-	-	2.430	2.466	2.416	2.541
0.2	HE_{11}	0.000	0.000	0.000	0.000	0.000	0.000	0.000
	TE_{01}	2.667	2.686	2.694	2.717	2.806	2.685	2.867
0.4	HE_{11}	0.766	0.780	0.786	0.784	0.820	0.876	1.200
	TE_{01}	2.821	2.868	2.890	2.884	3.001	2.844	3.056
0.6	HE_{11}	1.253	1.280	1.296	1.277	1.329	1.339	1.605
	TE_{01}	2.922	2.997	3.036	2.991	3.121	2.946	3.178

I: unperturbed step-index profile
II: inner-cladding dopants diffusion into the core [see (33)]
III: core dopants diffusion into the inner-cladding [see (32)]
IV: axial dip [see (36)]

The cutoffs are usually much less sensitive to small profile changes as can be seen in Table II where the HE_{11} and TE_{01} modes cutoff V-values are reported for the three kinds of deformation considered here.

C. Discussion

Following Section III-C we have computed, for the three examples under consideration, the shift $\delta\lambda_0$ in zero dispersion wavelength, and the variations $\delta a, \delta\Delta_1, \delta\Delta_2$ in fiber core radius and normalized index-differences needed individually to maintain $\lambda_0 = 1.55$ μm. The results are shown in Table III for $a_2 = 0.6a$, $a_1 = 1.2a$, $a_d = 0.5a$, and correspond to fibers having a HE_{11} mode spot-size equal to $\omega = 5$ μm; the structural parameters of these fibers are summarized in the upper part of Table I.

The change of zero dispersion wavelength remains small except in the case of a dip with $\sigma = 0.4$ and 0.6; if $\sigma = 0$ (singly-clad fiber), the shift has a sign and order of magnitude in agreement with other published results [3]. The values of $\delta\Delta_1$, $\delta\Delta_2$, and δa required to maintain λ_0 at $\lambda_0 = 1.55$ μm are in general smaller than the routine accuracy achievable during the preform fabrication or fiber pulling. These small values are due both to the small effect of diffusion or axial dip and to the large sensitivity to a parameter change.

Two conclusions of practical interest can thus be drawn.

1) Since the diffusion, which most occurs during fiber pulling, has not a large influence, fiber propagation characteristics can be predicted from a profile measured on preform. Note that a quick and highly accurate procedure of preform profiling is now available. For more details we refer the reader to [23].

2) In practice, the effect of axial dip cannot easily be compensated by a change of parameter because of the limited accuracy in parameter control; the best solution is then to reduce the dip by using $GeCl_4$ when collapsing the preform.

Lastly, not that the 1 or 2 ps/(km · nm) variation involved here can make the theoretical bandwidth X length product fall from about 3.10^3 GHz · km to 40-75 GHz · km. Note also that, near zero chromatic dispersion, the polarization mode dispersion should also be considered [24].

TABLE III

CHANGE IN STRUCTURAL PARAMETERS Δ_1, Δ_2, a REQUIRED TO MAINTAIN ZERO DISPERSON AT $\lambda_0 = 1.55\ \mu$m IN CASE OF DEFORMATION I, II, III (AS DESCRIBED BELOW) AND SHIFT $\delta\lambda_0$ IN ZERO DISPERSION WAVELENGTH IN CASE OF UNCHANGED Δ_1, Δ_2, a. THE HE_{11} MODE SPOT-SIZE IS EQUAL TO $\omega = 5\ \mu$m AND THE STRUCTURAL PARAMETERS OF THESE FIBERS ARE SUMMARIZED IN THE UPPER PART OF TABLE I. $\delta\Delta_1$, $\delta\Delta_2$ ARE EXPRESSED IN PERCENTS AND δa, $\delta\lambda_0$ IN MICRONS.

σ	0.			0.2			0.4			0.6		
	I	II	III	I	II	III	I	II	III	I	II	III
$\delta\Delta_1$	0.0	+ 0.04	+ 0.08	0.0	- 0.003	- 0.01	+ 0.004	+ 0.006	+ 0.02	+ 0.008	+ 0.007	+ 0.025
$\delta\Delta_2$	-	-	-	0.0	- 0.001	- 0.004	+ 0.005	+ 0.007	+ 0.02	+ 0.02	+ 0.014	+ 0.06
δa	0.0	- 0.07	- 0.14	0.0	- 0.004	- 0.02	+ 0.02	+ 0.02	+ 0.07	+ 0.04	+ 0.04	+ 0.15
$\delta\lambda_0$	0.0	- 0.01	- 0.02	0.0	- 0.002	- 0.009	+ 0.03	+ 0.05	+ 0.14	- 0.09	- 0.09	- 0.27

I: inner-cladding dopant diffusion into the core with $a_2 = 0.6a$ [see (32)]
II: core dopant diffusion into the inner-cladding with $a_1 = 1.2a$ [see (32)]
III: axial dip with $a_d = 0.5a$ [see (36)]

V. CONCLUSION

Optimum structural parameters for dispersion free fibers were considered; the choice between possible sets of parameters was made by considering the HE_{11} mode spot-size and the sensitivity of dispersion to any variation in the fiber geometrical characteristics. It was shown that singly-clad structures are less sensitive to changes in index-differences or core radius than structures with a depressed inner-cladding, but are more sensitive to a wavelength variation; however, they require high index-differences which induce an enhanced fiber attenuation. Structures with depressed inner-cladding allow smaller index-differences, but for a nonzero fundamental mode cutoff, the dispersion becomes very sensitive to geometrical characteristics. The tolerance requirements we have deduced in various cases are in general more severe than the 10 and 5 percent routine control on index-differences and core radius. Tolerance calculations based on loss criteria will be reported in a forthcoming paper.

The effects of dopant diffusion and axial dip on dispersion were investigated and found to be small. It would theoretically be possible to compensate these two effects by a slight change of geometrical fiber characteristics; this is, however, not easily feasible in practice because of the limited parameter control during fabrication. As for the axial dip, the best solution would be to diminish it by collapsing the preform in $GeCl_4$ vapor. The dopant diffusion during fiber pulling seems difficult to suppress; since it has only a small effect, fiber propagation characteristics may be accurately obtained from profile measured on preforms.

ACKNOWLEDGMENT

We gratefully acknowledge M. Monerie for instigating the work and fruitful discussions and J. C. Simon for comments on the manuscript.

REFERENCES

[1] H. Murata and N. Inagaki, "Low-loss single-mode fiber development and splicing research in Japan," *IEEE J. Quantum Electron.*, vol. QE-17, pp. 835–849, June 1981.
[2] T. Miya, Y. Terunuma, T. Hosaka, and T. Miyashita, "Ultimate low-loss single-mode fiber at 1.55 μm," *Electron. Lett.*, vol. 15, pp. 106–108, Feb. 1979.
[3] N. Imoto, A. Kawana, S. Machida, and H. Tsuchiya, "Characteristics of dispersion free single-mode fiber in the 1.5 μm wavelength region," *IEEE J. Quantum Electron.*, vol. QE-16, pp. 1052–1058, Oct. 1980.
[4] L. Cohen, W. L. Mammel, and S. Lumish, "Dispersion and bandwidth spectra in single-mode fibers," *IEEE J. Quantum Electron.*, vol. QE-18, pp. 49–53, Jan. 1982.
[5] B. J. Ainslie, K. J. Beales, C. R. Day, and J. D. Rush, "Interplay of design parameters and fabrication conditions on the performance of monomode fibers made by MCVD," *IEEE J. Quantum Electron.*, vol. QE-17, pp. 854–857, June 1981.
[6] J. Irven, A. P. Harrison, and C. R. Smith, "Long wavelength performance of optical fibers co-doped with fluorine," *Electron. Lett.*, vol. 17, pp. 3–5, Jan. 1981.
[7] L. G. Cohen and W. L. Mammel, "Tailoring the shapes of dispersion spectra to control bandwidths in single-mode fibers," presented at the 7th ECOC, Sept. 1981, paper 3.3.
[8] T. Miya, K. Okamoto, Y. Ohmori, and Y. Sasaki, "Fabrication of low dispersion single-mode fibers over a wide spectral range," *IEEE J. Quantum Electron.*, vol. QE-17, pp. 858–861, June 1981.
[9] S. Kawakami and S. Nishida, "Perturbation theory of a doubly-clad optical fiber with a low-index inner cladding," *IEEE J. Quantum Electron.*, vol. QE-11, pp. 130–138, Apr. 1975.
[10] D. Gloge, "Weakly guiding fibers," *Appl. Opt.*, vol. 10, pp. 2252–2258, Oct. 1971.
[11] A. W. Snyder and W. R. Young, "Modes of optical waveguides," *J. Opt. Soc. Amer.*, vol. 68, pp. 297–309, Mar. 1978.
[12] I. P. Kaminow and H. M. Presby, "Profile synthesis in multicomponent glass optical fibers," *Appl. Opt.*, vol. 16, pp. 108–112, Jan. 1977.
[13] P. M. Morse and H. Feshbach, *Methods of Theoretical Physics*, New York: McGraw-Hill, 1953, pp. 1112–1114.
[14] W. A. Gambling, H. Matsumura, C. M. Ragdale, "Zero total dispersion in graded-index single-mode fibers," *Electron. Lett.*, vol. 15, pp. 474–476, July 1979.
[15] M. J. Adams, *An Introduction to Optical Waveguides.* Chichester: Wiley, 1981.
[16] D. Marcuse, "Loss analysis of single-mode fiber splices," *Bell. Syst. Tech. J.*, vol. 56, pp. 703–718, May 1977.
[17] ——, "Gaussian approximation of the fundamental modes of graded fibers," *J. Opt. Soc. Amer.*, vol. 68, pp. 103–109, Jan. 1978.
[18] L. Jeunhomme, "Single mode fiber design for long haul transmission," *IEEE J. Quantum Electron.*, vol. QE-18, pp. 727–732, Apr. 1982.
[19] L. G. Cohen, W. L. Mammel, and S. Lumish, "Dispersion and bandwidth spectra in single-mode fibers," *IEEE J. Quantum Electron.*, vol. QE-18, pp. 49–53, Jan. 1982.
[20] A. W. Snyder and R. A. Sammut, "Fundamental (HE_{11}) modes of graded optical fibers," *J. Opt. Soc. Amer.*, vol. 69, pp. 1663–1671, Dec. 1979.
[21] A. Matsumura and T. Suganuma, "Normalization of single-mode fibers having an arbitrary index profile," *Appl. Opt.*, vol. 19, pp. 3151–3158, 1980.

[22] R. A. Sammut and C. Pask, "Simplified numerical analysis of optical fibers and planar waveguides," *Electron. Lett.*, vol. 17, pp. 105-106, Feb. 1981.
[23] P. L. Francois, I. Sasaki, and M. J. Adams, "Practical three-dimensional profiling of optical fiber preforms," *IEEE J. Quantum Electron.*, vol. QE-18, pp. 524-535, Apr. 1982.
[24] D. N. Payne, A. J. Barlow, and J. J. Ramskov-Hansen, "Development of low- and high-birefringence optical fibers," *IEEE J. Quantum Electron.*, vol. QE-18, pp. 477-488, Apr. 1982.

Pierre-Luc Francois, for a photograph and biography, see p. 380 of the April 1982 issue of this TRANSACTIONS.

Single-Mode Fiber OTDR: Experiment and Theory

DAN L. PHILEN, IAN A. WHITE, JANE F. KUHL, AND STEPHEN C. METTLER

Abstract—**An OTDR measurement technique with an end detection dynamic range of 63 dB is described for use with single-mode fibers. A theoretical analysis of single-mode fiber backscattering is presented which predicts loss penalties in single-mode OTDR's compared with multimode fibers. The prediction of the critical power levels of about 3-4 W for the onset of nonlinear effects in fibers is shown to be in good agreement with experiment. Fusion welded splices do not demonstrate significant backscattered power.**

INTRODUCTION

In all optical communications systems there is a need to examine the transmission medium, after it is installed, for fault location and for determination of the characteristics of the medium in a field environment. In the factory most of the transmission medium parameters are determined by a two-point technique since both ends of the line are accessible. In a field situation, however, it is not always practical to have access to both ends of the transmission medium. Time domain reflectometry was developed for conventional copper wire transmission systems to overcome this problem and can also be applied to optical transmission media.

Two early papers on optical time domain reflectometry (OTDR) [1], [2] outline the basic approach. A short pulse of light is launched into the fiber and the backscattered signal is monitored as a function of time (or equivalently, distance) along the fiber. The magnitude of the backscattered signal is dependent on the Rayleigh scattering, attenuation, imperfections and splices, and optical power level in the fiber. OTDR can, therefore, be used to measure attenuation and splice loss, and for fault location. For multimode fibers the attenuation and splice loss measurements are complicated by the uncertainty in the modal power distribution of the backscattered signal, as well as the variation in scattering levels of the fibers on either side of the splice. Typically, at 0.825 μm, the length of fiber that can be examined is about 5 km.

As interest shifts to longer wavelengths and single-mode fibers, the range of OTDR measurements must be increased dramatically. The lower loss of long wavelength fibers together with the high data rate of single-mode fibers make possible repeaterless spans of fiber in excess of 40 km, which must be examined during and after installation. For single-mode fibers, attenuation and splice loss measurements are potentially more reliable than in multimode fibers since the backscattered information is contained in only one propagating mode.

In this paper we present a theoretical analysis of OTDR for single-mode fibers which corrects previously published work and indicates important considerations in the design of such an OTDR measurement system. Experimental verification of the predictions of the onset of nonlinear effects are presented and a single-mode OTDR which can detect the end of 30 km of fiber with one-way loss of 1.1 dB/km is demonstrated.

Before a detailed discussion of the results of this paper, the recent rapid progress of single-mode OTDR necessitates a review of previous work.

OVERVIEW

Recently, a theoretical treatment of backscattering in single-mode fibers was presented [3], and shortly thereafter, several papers were published on experimental results of single-mode OTDR [4]-[6]. Two of the experimental papers [4], [5] used a modified avalanche photodiode (APD) operating as a photon counter and a diode laser operating at 0.85 μm. Only a single channel of the photon counter was used for signal acquisition with a fault signified by a sudden increase in the dwell time of the photon counter. Attenuation or splice loss measurements using this method were not demonstrated. A third experimental paper [6] used a Q-switched Nd:YAG laser operating at 1.06 μm as the source. A higher power laser source was necessary to overcome the additional loss penalties not found in multimode OTDR's.

One design problem with OTDR's is to couple a large amount of power into a fiber while preventing saturation of the detector with the Fresnel reflection from the fiber end face. Virtually all OTDR schemes attempt to minimize this effect. The scheme used in [6] couples the input power through a twisted multi-

Manuscript received March 15, 1982; revised May 12, 1982.
The authors are with Bell Laboratories, Norcross, GA 30071.

0018-9480/82/1000-1487$00.75